

# $\rho_T$ Production via $W_L Z_L$ Fusion at Hadronic Colliders

S.R. Slabospitsky  
*Institute for High Energy Physics,  
Protvino, Moscow Region, 142284 Russia*  
slabospitsky@mx.ihep.su

G. Azuelos  
*Université de Montreal, Canada*  
azuelos@lps.Umontreal.ca

## Abstract

Multiscale technicolor models predict the existence of high mass resonances at hadron colliders. Although the quark fusion process of production dominates, vector boson fusion offers the advantage of allowing forward jet tagging for background suppression. We calculate here the cross section and differential distributions for  $\rho_T$  production in the vector boson fusion channel at the LHC.

# 1 Introduction

In the search for the origin of electroweak symmetry breaking, strong coupling models are an alternative to the Standard Model Higgs mechanism, or for weakly coupled theories based on supersymmetry. Although classical technicolor[1] suffers from major shortcomings, viable multiscale models have been developed [2] which allow for fermion mass generation and for the absence of weak neutral currents. These models, which are not necessarily excluded by precision measurements of electroweak parameters at LEP and SLC [3], not only provide the technipions which serve as the longitudinal components of the gauge bosons, but also predict the existence of technipions ( $\pi_T$ ) as mass eigenstates, as well as technirhos ( $\rho_T$ ), and other techniparticles.

The feasibility of observing such resonances produced in  $q\bar{q}$  fusion, in ATLAS has been reported in [4]. The analysis was based on a PYTHIA [5] implementation of the multiscale model of Eichten, Lane and Womersley [2], and took into account detector effects by using a fast simulation of the ATLAS detector. In particular, one of the channels analyzed was  $\rho_T^\pm$  production with subsequent decay into  $\pi_T^0 W_L^\pm \rightarrow b\bar{b}\ell^\pm\nu$ . Assuming a quark fusion process, the authors [2] of the model have calculated the relevant matrix elements. It has then been shown in [4] that, given some reasonable values for the parameters of the model, the observation of such a process should be feasible with ATLAS, but is limited by background for possible large masses of  $\rho_T$  and  $\pi_T$ .

The technique of forward jet tagging has been shown [4] to be very powerful in eliminating backgrounds from such processes as  $W + \text{jets}$  production. For that reason, it is important to estimate if  $\rho_T$  production via a vector boson fusion process can be a useful complementary channel for discovery of such a resonance. We evaluate here the cross section for this process.

The article is organized as follows. First, the model for the form factor and decay width of  $\rho_T$  are presented in section 2. Results on the cross section calculation are given in section 3. The main results are summarized in the conclusion.

## 2 Model

In this section we describe in detail the essential features of the model used in our calculations.

The lighter isotriplet  $\rho_T$  is assumed to decay dominantly into pairs of the mixed state of isotriplet  $|\Pi_T\rangle = \sin\chi|W_L\rangle + \cos\chi|\pi_T\rangle$ , where the value of the mixing angle  $\chi$  is assumed [2] to be:  $\sin\chi = 1/3$ . The vertex  $\rho_T \rightarrow \pi_A\pi_B$ , where  $\pi_{A,B}$  may be longitudinal  $W_L^\pm, Z_L$  bosons or technipion  $\pi_T$ , has the following form [2]:

$$g_\rho F_{\rho\pi\pi}(p, q_A, q_B) C_{AB} \varepsilon^\nu(q_A - q_B)_\nu \quad (1)$$

where  $p, q_A$  and  $q_B$  are the momenta of  $\rho_T, \pi_A$  and  $\pi_B$ ;  $\varepsilon^\nu$  is the polarization vector of  $\rho_T$ ; the parameters  $C_{AB}$  are equal to

$$C_{AB} = \begin{cases} \sin^2\chi & \text{for } W_L^\pm Z_L, \\ \sin\chi\cos\chi & \text{for } W_L^\pm \pi_T, \\ \cos^2\chi & \text{for } \pi_T \pi_T \end{cases} \quad (2)$$

and  $g_\rho$  is a coupling constant, normalized as follows [2]:

$$\frac{g_\rho^2}{4\pi} = 2.91 \left( \frac{3}{N_{TC}} \right),$$

where  $N_{TC} = 4$  (see [2]).

Being a compound object, consisting of two heavy techniquarks, the technirho couples to two technipions (or longitudinal  $W, Z$  bosons) by means of the diagram in Fig.1. In the loop the techniquarks 1 and 2 are on-shell (it is a typical approximation for a such consideration), while quark 3 is virtual. The latter has a momentum  $p_3$  given by:

$$p_3 = p_1 - q_A = \frac{1}{2}p_\rho - q_A = \frac{1}{2}(q_B - q_A).$$

The production vertex is naturally suppressed by large virtualities of the  $W_L$  and  $Z_L$ , but is enhanced, in that case, by large values of  $p_3$  in the numerator. To be consistent with the Effective W Approximation (EWA), the additional form factor  $F_{\rho\pi\pi}(p, q_A, q_B)$  in (1) is introduced.

$$F_{\rho\pi\pi}(p, q_A, q_B) = \frac{M_\rho^2 - M_{\pi_A}^2 - M_{\pi_B}^2}{2(q_A q_B)}, \quad (3)$$

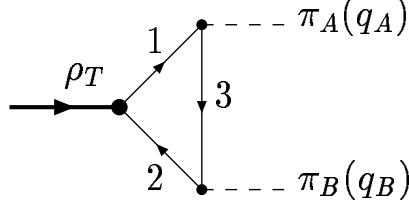


Figure 1: Diagram describing  $\rho_t \pi_A \pi_B$  coupling via a loop of heavy techniquarks (lines 1, 2, and 3). The quarks  $Q_1$  and  $Q_2$  are on-shell ( $p_{Q_1} = -p_{Q_2} = \frac{1}{2}p_\rho$ , and the momentum of the off-shell quark  $Q_3$  is  $\frac{1}{2}(q_B - q_A)$ ).

where  $M_\rho, M_{\pi_{A,B}}$  are the masses of  $\rho_T, \pi_{A,B}$ . In analogy with the case of a heavy  $(Q_1 \bar{Q}_2)$ -meson, this form-factor takes into account the possible off-shellness of technipions  $\pi_A$  and  $\pi_B$ . The denominator in the effective  $\rho_T \pi_A \pi_B$  vertex (3) results from the propagator of this virtual quark in the loop:

$$m_3^2 - p_3^2 = \frac{M_\rho^2}{4} - \frac{(q_B - q_A)^2}{4} = (q_A q_B), \quad (4)$$

where  $M_\rho^2 = q_A^2 + q_B^2 + 2(q_A q_B)$ .

In the decay vertex of  $\rho_T$ , for on-shell technipions  $\pi_A$  and  $\pi_B$ , we have  $F_{\rho\pi\pi}|_{\text{on-shell}} = 1$ .

Using the vertex (1) we get the well-known equation for the  $\rho_T \rightarrow \pi_A \pi_B$  decay width [2]:

$$\Gamma(\rho_T \rightarrow \pi_A \pi_B) = \frac{2\alpha_{\rho_T} C_{AB}^2 p_{AB}^3}{3 M_\rho^2} \quad (5)$$

We investigate the case of  $\rho_T^\pm$  production with its subsequent decay into  $\pi_T^0 W_L^\pm$  pair. The corresponding branching ratio has a non-trivial behavior, as can be seen in Fig.2 for three decay channels of the charged technirho:  $\rho_T^\pm \rightarrow \pi_T^0 \pi_T^\pm$ ,  $\rho_T^\pm \rightarrow \pi_T^0 W_L^\pm + \pi_T^\pm Z_L$  or  $\rho_T^\pm \rightarrow Z_L W_L^\pm$ .

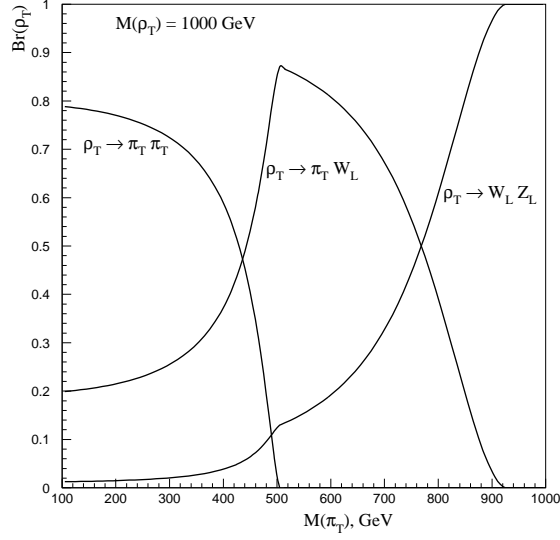


Figure 2: Branching ratios versus  $M_{\pi_T}$  for the decay channels of  $\rho_T^\pm \rightarrow \pi_T^0 \pi_T^\pm$ ,  $\rho_T^\pm \rightarrow \pi_T^0 W_L + \pi_T^\pm Z_L$  or  $\rho_T^\pm \rightarrow Z_L W_L^\pm$ . We consider the case  $m_{\rho_T} = 1$  TeV and  $m_{\pi_T} = 500$  GeV.

We can distinguish two regions in the technipion to technirho mass ratio. In the first region, namely  $M_{\pi_T}/M_{\rho_T} \leq 1/2$ , the  $\rho_T^\pm \rightarrow \pi_T \pi_T$  decay is kinematically allowed. As  $M_{\pi_T}$  increases (keeping  $M_{\rho_T}$  fixed) the relative momentum  $p_{AB}$  in equation (5) decreases. As a result we have a decreasing branching fraction for the  $\pi_T \pi_T$  channel, while the other two channels increase in their relative value (see Fig. 2). Just above the value  $M_{\pi_T}/M_{\rho_T} = 1/2$  the branching ratio for the  $\pi_T W_L$  channel reaches its maximum value. As the mass of  $\pi_T$  rises further, in the second region up to the kinematic bound  $M_{\pi_T}/M_{\rho_T} = 1$ , the relative boson momentum  $p_{W\pi_T}$  decreases, yielding a decreasing branching ratio for technipion + longitudinal  $W$  boson.

### 3 Calculation of the cross section

We examine the reaction of technirho production at  $\sqrt{s} = 14$  TeV (LHC collider) with subsequent decay of the technirho into a neutral technipion  $\pi_T^0$  and a longitudinal  $W_L^\pm$ -boson

$$pp \rightarrow q_f q_f \rho_T (\rightarrow \pi_T^0 W_L) X \quad (6)$$

Since each of the final particles from the  $\rho_T$  decay has a very narrow width in comparison with its mass, we take both the final  $W_L$ -boson and technipion to be on-shell.

One of the diagrams describing the subprocess

$$qq' \rightarrow q_f q'_f \rho_T \rightarrow q_f q'_f \pi_T^0 W_L \quad (7)$$

is shown in Fig. 3. Only fusion of longitudinal  $W_L$  and  $Z_L$  bosons, radiated from the initial quarks  $q$  and  $q'$ , needs to be taken into account.

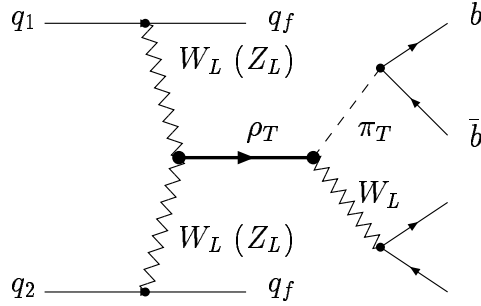


Figure 3: One of the diagrams describing  $\rho_T^\pm$  production with subsequent decay into  $\pi_T^0 (\rightarrow b\bar{b})$  and  $W_L^\pm (\rightarrow l^\pm \nu)$ .

The polarization vector of a longitudinal boson with mass  $M$  and 4-momentum  $q$  is equal to [6];

$$e^\nu = \frac{q^\nu}{M} + \frac{(q_0 - |\vec{q}|)}{M} (-1, \vec{q}/|\vec{q}|). \quad (8)$$

In our calculations we set that

$$\begin{aligned} \text{BR}(\pi_T^0 \rightarrow b\bar{b}) &= 1, \\ \text{and } \text{BR}(W_L^\pm \rightarrow l^\pm \nu) &= 1/9. \end{aligned}$$

We use the CTEQ2L parameterization of the proton structure functions [7]. For evolution scale we set  $\sqrt{Q^2} = M_W$ .

The resulting cross sections for different values of the masses of  $\rho_T^\pm$  and  $\pi_T^0$  are presented in the Table 1. Note that the cross section of the reaction (6) may be presented in the factorized form as follows:

$$\sigma(pp \rightarrow q_f q_f \rho_T (\rightarrow \pi_T^0 W_L) X) = \sigma(pp \rightarrow q_f q_f \rho_T X) \times \text{BR}(\rho_T \rightarrow \pi_T^0 W_L). \quad (9)$$

Therefore, the  $M_{\pi_T}$ -dependence of the cross section for reaction (6) with a given value of  $M_{\rho_T}$  is completely determined by the branching ratio of technirho decay into  $\pi_T W_L$  (see Fig.2). In particular, we expect that the cross section of reaction (6) should reach a maximum for  $M_{\pi_T}/M_{\rho_T} \approx 1/2$ .

A brief remark about the role of the form-factor  $F_{\rho\pi\pi}$  in the  $\rho_T \pi_A \pi_B$  vertex (1) is in order. In Fig.4 comparison is made of the pseudorapidity distribution of the final primary light quarks  $q_f, q'_f$  (not from  $\pi_T^0$  decay). The dashed histogram corresponds to the  $q_W$  and  $q_Z$  dependent form-factor  $F_{\rho\pi\pi}$  using expression (3), while the solid histogram is produced with  $F_{\rho\pi\pi} = 1$ . From this figure one clearly sees that the latter choice ( $F = 1$ ) disagrees with expectations from the effective  $W$ -approximation, since the pseudorapidity distribution of the final  $q_f$  do not peak in the forward and backward direction).

Other differential distributions are shown in the Figs. 5-6 (solid histograms).

We also compare our exact results with the calculations within effective  $W$ -approximation approach [6]. In this case the matrix element for the process

$$W_L Z_L \rightarrow \rho_T \rightarrow \pi_T W_L$$

looks very simple. The exact form of the  $|M|^2$  is presented below

$$\begin{aligned} |M|^2 &\propto C_{WZ}^2 C_{\pi W}^2 \left( \frac{(p_w^2 - p_z^2)(p_a^2 - p_b^2)}{M_{\rho_T}^2} - (p_w - p_z)(p_a - p_b) \right)^2 \\ &\times \frac{1}{(P_{\rho_T}^2 - M_{\rho_T}^2)^2 + (\Gamma_{\rho_T} M_{\rho_T})^2}, \end{aligned}$$

where  $p_w$  and  $p_z$  are the momenta of the initial  $W_L$  and  $Z_L$ , while  $p_a$  and  $p_b$  are the momenta of the final longitudinal  $W_L$  boson and technipion  $\pi_T$ , respectively (see [8], for detail). The parameters  $C_{WZ}$  and  $C_{\pi W}$  are given by the equation (2).

The corresponding differential distributions are shown in the Figs. 5-6 (dashed histograms). One can see from these figures that the shapes from the exact and EWA calculations are in good agreement.

As an example for the above calculation, the same case as in [4] but by the process of gauge boson fusion, has been reported in [9]:  $\rho_T^\pm \rightarrow qqW^\pm\pi_T^0 \rightarrow l\nu b\bar{b}$  (where  $l$  is an electron or muon), with  $m_{\rho_T} = 800$  GeV and  $m_{\pi_T} = 500$  GeV. For this process,  $\sigma \times BR$  is about 2.2 fb, as can be seen from table 1 (accounting for both  $\mu\nu$  and  $e\nu$  decays of the charged  $W$ ). This cross section depends sensitively on the assumed value of the mixing  $\sin\chi$  between the longitudinal gauge bosons and the technipions since it involves the  $WZ\rho_T$  vertex as well as the  $\rho_TW\pi_T$  vertex. It was shown that, with the same model parameters, the resulting signal would leave about 2.6 events on a background of about 5.6 for an integrated luminosity of  $30 \text{ fb}^{-1}$ , or a value of  $\sigma/\sqrt{B} = 1.1$ . This is to be compared with a significance of 2.1 obtained in ref [4] for the  $q\bar{q}$  fusion contribution. This process of vector boson fusion with forward tagging of jets could therefore complement the  $q\bar{q}$  fusion process, but would not be a discovery channel unless the  $\sigma \times BR$  is at least 12 fb.

## 4 Conclusion

We have calculated the cross section and differential distributions for  $\rho_T$  production, in the vector boson fusion channel. We have compared our exact calculations with those within the effective W-boson approximation. The shapes of the differential distributions for the final particles (charged leptons and  $b$ -quarks) obtained by the two methods (the exact and EWA) are in reasonable agreement.

For a particular choice of masses for the technirho and technipion ( $M_{\rho_T} = 800$  GeV and  $M_{\pi_T} = 500$  GeV) the possibility of extracting the signal from the background was evaluated. After applications of kinematical cuts, assuming low luminosity, one would expect about 2.6 events from the signal and about 5.6 ones from the background. Therefore, the process of vector boson fusion with forward tagging of jets could complement the  $q\bar{q}$  fusion process.



## Acknowledgments

We thank to D. Froidevaux, R. Mazini, A. Miagkov, V. Obraztsov, and A. Zaitsev for fruitful discussions. S.S. acknowledges the hospitality of Theory Division of CERN, where this work had complete.

## References

- [1] S. Dimopoulos and L. Susskind, *Nucl. Phys.* **B155** (1979) 237;  
E. Eichten and K. Lane, *Phys. Lett.* **B90** (1980) 125
- [2] E. Eichten and K. Lane, *Phys. Lett.* **B388** (1996) 803;  
E. Eichten, K. Lane and J. Womersley, *Phys. Lett.* **B405** (1997) 305.
- [3] K. Lane, hep-ph/9409304;  
M. Knecht and E. de Rafael, *Phys. Lett.* **B424** (1998) 335
- [4] Detector and Physics Performance Technical Design Report, CERN publication, LHCC 99-14/15
- [5] T. Sjöstrand, *Comp. Phys. Comm.* **82** (1994) 74.
- [6] Dawson S., *Nucl. Phys.* **B249** (1985) 42;  
Duncan M.J., Kane G.L., and Repko W.W., *Nucl. Phys.* **B272** (1986) 517.
- [7] Wu-Ki Tung, "*Perspectives in Global QCD Analyses*", Proc. of the Int. Workshop of DIS and Related Subjects, Eilat, Israel (1994), ed. A.Levy, World Scientific Publishing Co., Singapore.
- [8] Pirogov R.Y., Diploma Thesis, Moscow Institute of Physics and Technology, 1999, Moscow.
- [9] G. Azuelos, R. Mazini and S.R. Slabospitsky, ATLAS note ATL-PHYS-99-021.

Table 1:

The value of the  $\rho_T \rightarrow \pi_T^0 W_L^\pm$  production cross sections (times branching ratios for  $\pi_T^0 \rightarrow b\bar{b}$  and  $W_L^\pm \rightarrow \mu^\pm \nu$ ) for different values of  $M_{\rho_T}$  and  $M_{\pi_T}$ . The masses are in GeV, while the cross sections are in fb.

$pp \rightarrow \rho_T^+ X$	$M_\pi = 200$	400	500	600	800	1000	1200	1400
$M_\rho = 400$	1.924							
500	0.630	0.268						
600	0.415	1.213	0.146					
800	0.247	0.752	0.690	0.610				
1000	0.107	0.135	0.307	0.296	0.163			
1200	0.088	0.079	0.079	0.281	0.172	0.077		
1500	0.105	0.057	0.038	0.075	0.079	0.089	0.038	0.001
2000	0.030	0.014	0.011	0.011	0.010	0.027	0.027	0.032
$pp \rightarrow \rho_T^- X$	$M_\pi = 200$	400	500	600	800	1000	1200	1400
$M_\rho = 400$	1.288							
500	0.391	0.166						
600	0.243	0.699	0.088					
800	0.129	0.399	0.378	0.319				
1000	0.060	0.072	0.162	0.155	0.087			
1200	0.050	0.040	0.042	0.148	0.087	0.038		
1500	0.060	0.030	0.019	0.036	0.038	0.042	0.019	0.001
2000	0.018	0.008	0.005	0.006	0.005	0.012	0.012	0.014

Table 2:

Signals and backgrounds for the observation of  $\rho_T^\pm \rightarrow W^\pm \pi_T^0 \rightarrow \ell^\pm \nu b \bar{b}$ . The last column shows the multiplicative factor used in the normalization of the background, assuming  $30 \text{ fb}^{-1}$ .

Process	preselection	$\sigma$ (pb)	Nb. of events simulated	factor $30 \text{ fb}^{-1}$
$\rho_T^\pm$	$\hat{m} > 600 \text{ GeV}/c^2$	0.0022	2000	0.033
$t\bar{t}$	$\hat{p}_T > 100 \text{ GeV}/c$	333	$5.3 \times 10^6$	1.88
W + jets	$W \rightarrow \ell \nu; \hat{p}_T > 100 \text{ GeV}/c$	638	$6 \times 10^6$	3.2
$W b \bar{b}$		19.9	$2 \times 10^5$	3.0
Z + jets	$Z \rightarrow \ell^+ \ell^-; \hat{p}_T > 100 \text{ GeV}/c$	85.5	$6 \times 10^5$	4.28
WZ		20.6	$10^6$	0.618

Table 3:

Number of signal/ $t\bar{t}$ /(W+jets+Z+jets) events around the mass peak of the signal, after the application of successive cuts (see the text). The last two lines give the  $\sigma \times BR$  predicted by the model, as well as the  $\sigma \times BR$  required for a  $5\sigma$  significance of the signal

Cut	$\rho_T$
A	6.2/3150/34.7
B	6.0/1400/29.7
C	2.6/5.6/0
$S/\sqrt{B}$	1.1
$\sigma \times BR$ (fb)	
model	2.5
for $5\sigma$ significance	11.6

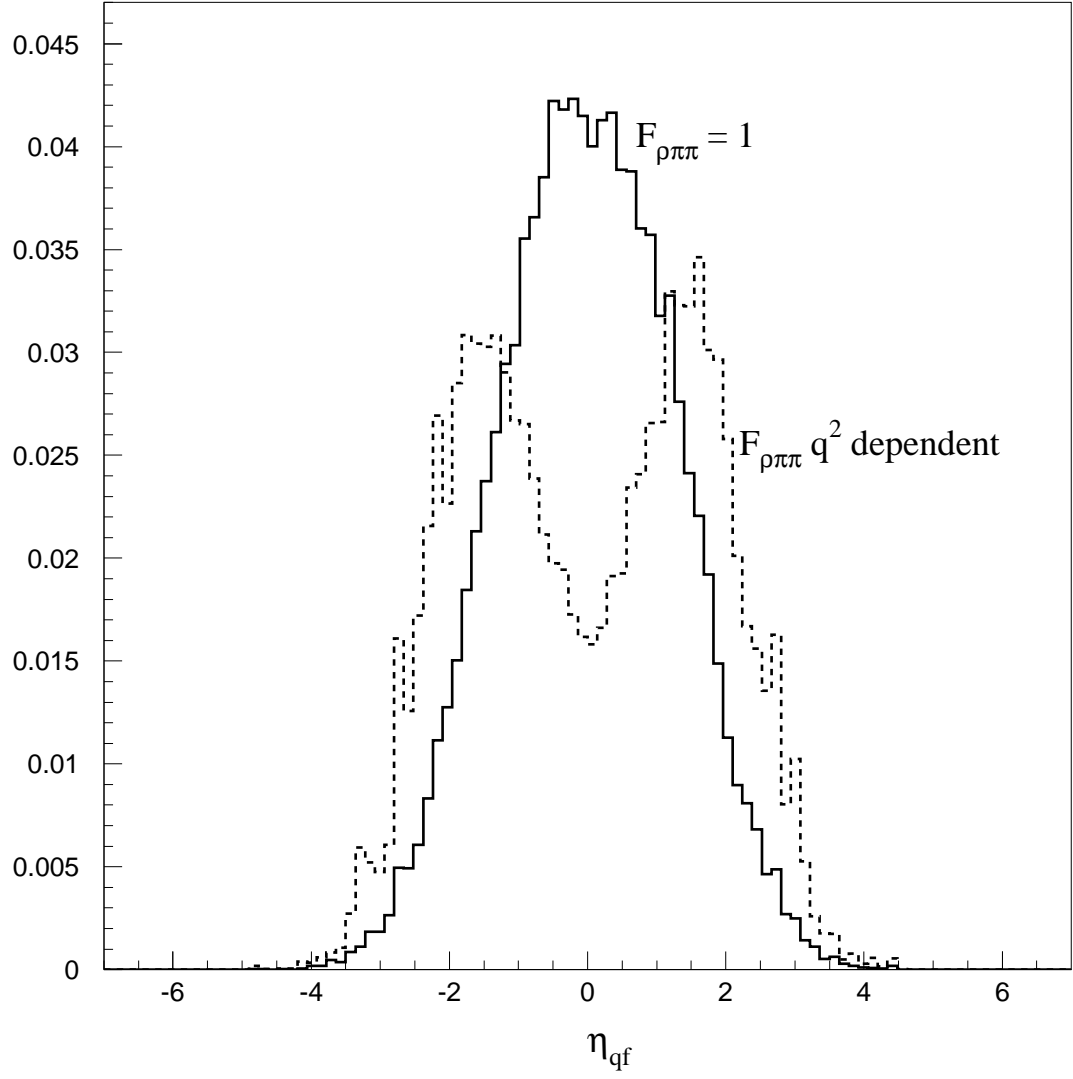


Figure 4: Pseudorapidity distribution of final  $q_f$  quarks, calculated with momentum-transfer dependent form-factor  $F_{\rho\pi\pi}$  of the form of equation (3) (dashed histogram) and with  $F_{\rho\pi\pi} = 1$  (solid histogram).

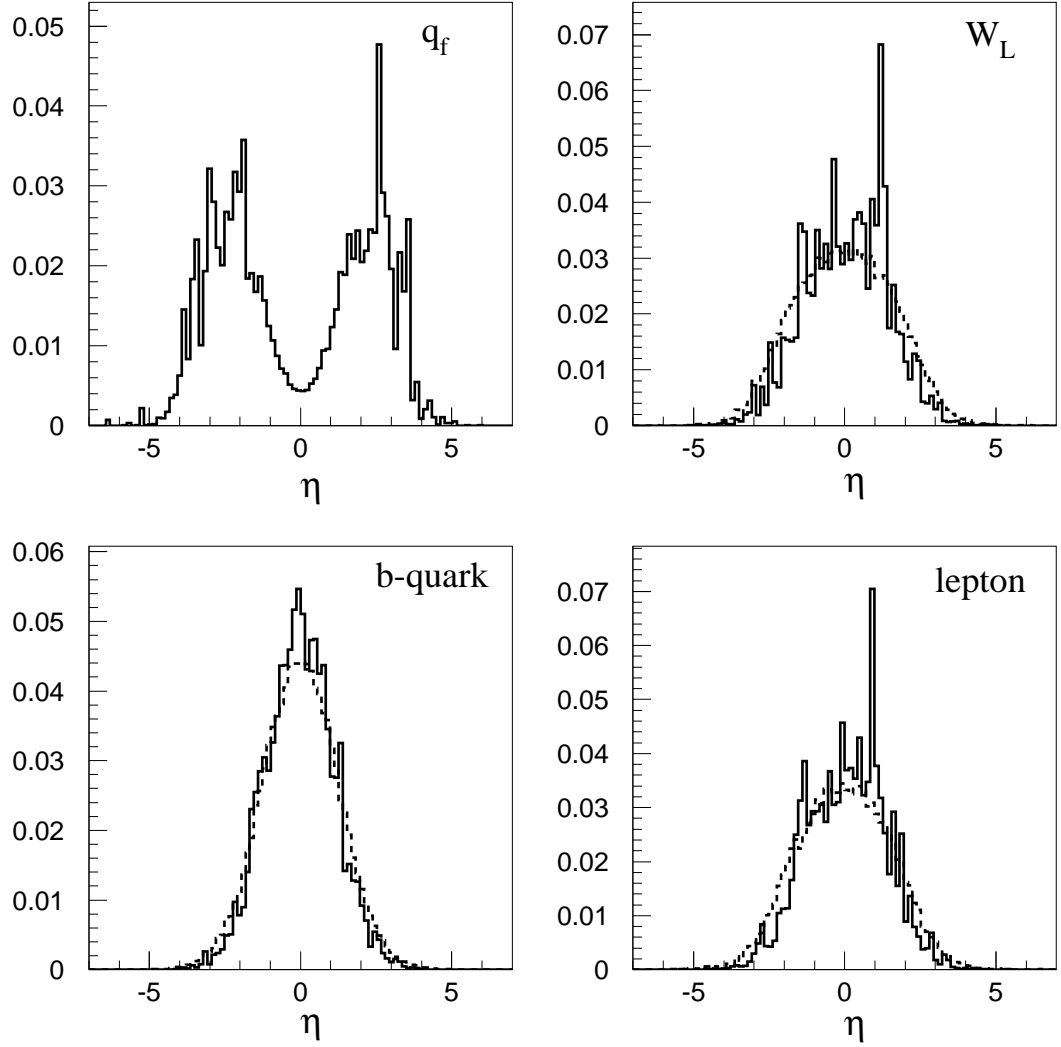


Figure 5: Pseudorapidity distributions of final particles, namely,  $q_f$  quarks,  $W_L$ ,  $b$ -quarks, and charged lepton. Solid and dashed histograms are the results of the exact and EWA calculations, respectively. All histograms are normalized to unit area.

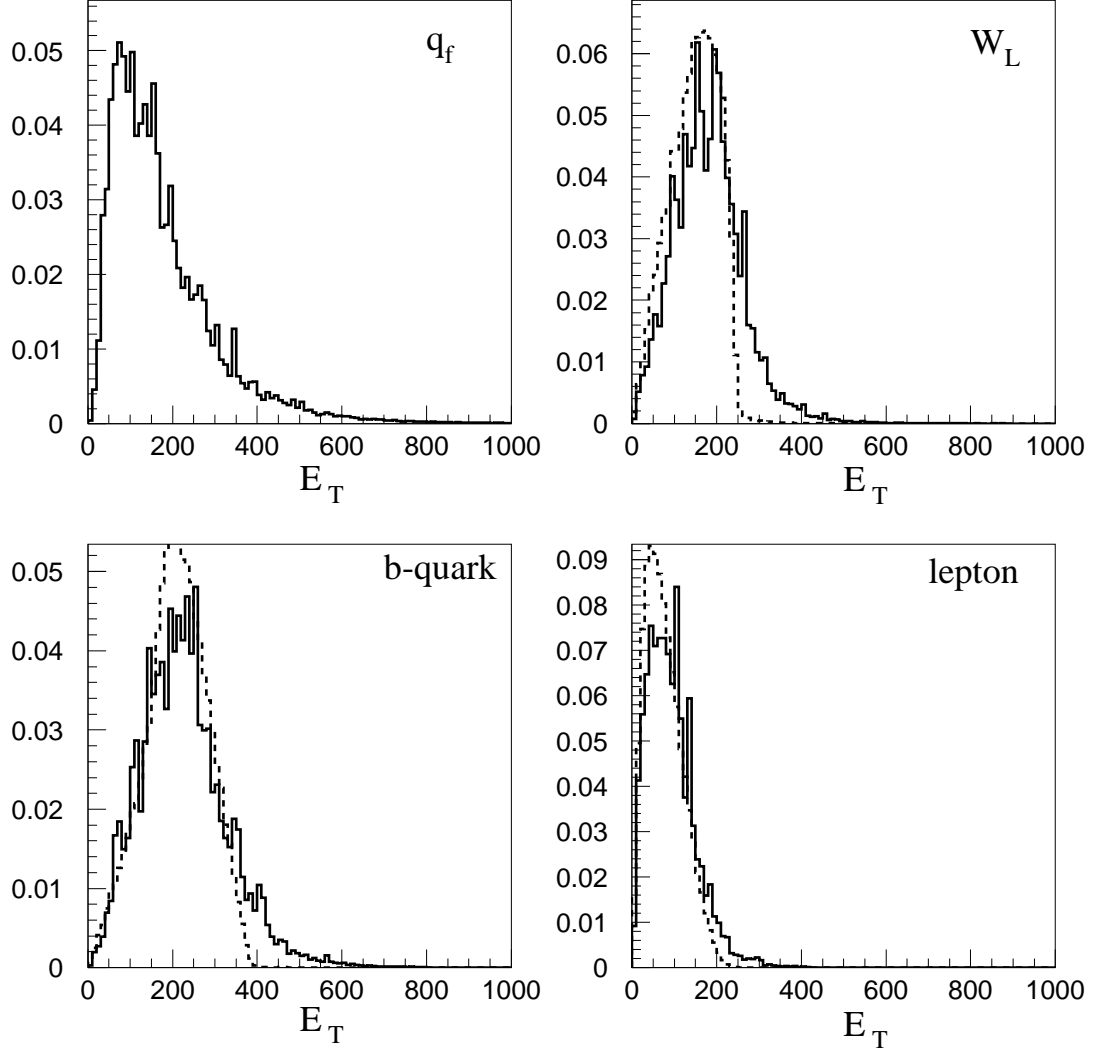


Figure 6: Transverse energy distributions of final particles, namely,  $q_f$  quarks,  $W_L$ ,  $b$ -quarks, and charged lepton. Solid and dashed histograms are the results of the exact and EWA calculations, respectively. All histograms are normalized to unit area.